Global Scientific JOURNALS

GSJ: Volume 12, Issue 1, January 2024, Online: ISSN 2320-9186

www.globalscientificjournal.com

Adsorption of Copper(II) Ions and Indigo Carmine Dye by Optimized Activated Carbon from Cocoa Pods

Mouafo Mouafo Franck Joel., Ankoro Odogu Naphtali., Kouotou Daouda., Lekene Ngouateu Rene., Benedoué Serge Arnold., Betga Alex Wordlight., Ndi Julius Nsami*., Ngomo Horace Manga.

Applied Physical and Analytical Chemistry Laboratory, Department of Inorganic Chemistry, Faculty of Science, University of Yaoundé I, P.O. Box 812, Yaoundé, Cameroon

*Corresponding author; e-mail: ndinsami2002@yahoo.com/bigpielo2002@yahoo.com

ABSTRACT

The optimization of the preparation of activated carbon from cacao pods was done according to Box-Behnken plan and the optimal conditions were resident time, impregnation ratio and temperature of 1hour, 1,3 and 333°C respectively. The activate d carbon was characterized using several methods such as BET-BJH, SEM, TGA-DSC, FTIR. The result obtained in batch mode show that the maximum adsorption capacity was observed at pH 2 and 4,5 for Indigo carmine dye and copper(II) ions. The adsorption capacity increases with increased concentration and decreases with increasing mass. The nonlinear regression plot of Indigo carmine and copper (II) ions show none of the model describe best the adsorption mechanism due to their low R^2 value. The kinetic model that describe the adsorption is Elovich for the two adsorbents with correlation coefficients of 0,98 and 0,99 close to unity for Indigo carmine dye and copper (II) ions respectively. The Fourier infra-red spectra (FTIR) before and after adsorption confirmed that the predominant mechanism for our adsorbent is chemisorption.

Keywords: optimization, cocoa pod, activated carbon, indigo carmine, copper(II) ions

INTRODUCTION

In recent decades, rapid industrialization and urbanization due to the growth of the population has caused significant water contamination, by an excessive production of large volumes of solid and liquid waste **(Zulfiqar et al., 2019)**. Due to high market demand, industries such as textiles, pharmaceuticals, metallurgical, petroleum, cosmetics, plastics industries, food and beverage, use a wide variety of dyes and metals **(Harrache et al., 2019)** and release them into nature generally without treatment. Most of these dyes are chemically and thermally stable, non-biodegradable and quite toxic **(Leon et al., 2018; Ahmadi et Ganjidoust., 2021)**. The polluted wastewater cause damages in the environment and also affect human's health with diseases such as carcinogenic and dysfunction of the kidneys. These is why the removal of organic dyes from wastewater remains an environment challenge for all the research community **(Li et al., 2016)**. Faced with this alarming situation, it is important to properly treat domestic wastewater before discharging it into the environment in order to avoid pollution of increasingly limited water resources and waterborne diseases. In order to reduce the presence of these pollutants such as copper (II) ions and indigo carmine dye in water, numerous methods are used, among which stand out chemical precipitation, ions exchanges, membrane filtration,

electrolytiques process, coagulation and floculation, inverse osmose and adsorption **(Ngaha et al.,2019; Ahmadi et Ganjidoust., 2021)**. Amount all these methods that adsorption is the one that is technically efficient, less expensive and it's use for the removal of wide range of contaminants **(Ankoro et al., 2020; Mashile et al., 2021; Rashid et al.,2021)**. It is one of the most widely used methods in the treatment of pollutants (dyes and heavy metals). Several materials have already been recovered for the manufacture of activated carbon. Much research has focused on the use of synthetic activated charcoal but its high cost remains the main disadvantage **(Athéba et al., 2015)**. To overcome this problem, many studies have investigated the possibility of applying agri-food wastes/by-products as they are available and inexpensive. From the economic point of view, adsorbents should be highly selective for pollutants, efficient and inexpensive, adsorption The use of these materials has a dual objective, that of manufacturing quality activated carbons at low cost from local materials and thus giving these same materials added value **(Ousmaila et al., 2016)**. Lately, numerous scientists have studied the possibility of using activated carbon derived nature or low cost agricultural wastes such as banana peel, orange peel, lemon peel, cassava peel, groundnuts shells, peanut shells, bamboo shoots, coconut shells, egusi shells and cocoa pod **(Wong et al., 2018; Hashem et al., 2020; Ahmadi and Ganjidoust., 2021; Jiang et al., 2021)**. One of the possible adsorbents is Cocoa pods because of their great abundance. an annual production of about 5,252,377 tonnes of beans in 2018 worldwide **(FAOSTAT, 2020)** and 335,850 tonnes in Cameroon **(DESA, 2020)**. This study is aimed at highlighting Adsorption of Copper(II) Ions and Indigo Carmine Dye by Optimized Activated Carbon from Cocoa Pods is to convert cocoa pods into activated carbon to remove pollutants such as indigo carmine and copper (II) in waters. Various techniques were used to characterize the prepared activated carbon Fourier-transform infrared spectroscopy (FTIR), scanning electron microscopy (SEM).

II-MATERIALS AND METHODS

II.1-Preparation of activated carbon

II.1.1-Choice of precursors

The raw material used for the preparation of our ACP is cocoa pod, a material containing cellulose, lignite and hemicellulose. It was collected in the Central Cameroon region more precisely in the Mfoundi division, Nkol-Afamba sub-division and Elat district on the East side of Yaoundé city. These cocoa pods constitute a large part of the harvest, but are not valued because they are of no use to farmers. They are therefore a real source of agricultural waste and whose transformation into activated charcoal will be an added value.

Figure 1: Cocoa pod

II.1.2-Preparation of activated carbon (Activation and Carbonization)

The preparation of the coal was carried out by chemical activation using the method of experimental designs and particularly the Box-Behnken design. The harvested pods are thoroughly washed under running water to remove impurities and then rinsed with distilled water. These pods are cut and then dried in the sun for three weeks. Once dried, these pods are crushed until particles with a size between 1.25 and 2.5 mm are obtained.

These particles are impregnated with orthophosphoric acid (H_3PO_4) with a desirable mass ratio (r) given by the relation

$$r = \frac{m_{cabosse}}{m_{H3PO4}} = 1.3$$

Once the impregnation is done, this debris will be dried in the oven for 24 hours at a temperature of 110° C. The carbonization of our material was done at different temperatures and residence times with a constant heating rate of 10 °C/ min and the cooling was done gradually until room temperature. Once cooled, the coal is washed with distilled water until a neutral pH is obtained. The coal obtained is put in the oven for 24 hours at 110 ° C. The dried coal is weighed and crushed in a porcelain mortar using a pestle and then sieved until the powder size < 75 µm is obtained. The powder obtained is kept in a jar and then put in the desiccator

II.2-Optimization and characterization of activated carbon preparation

II.2.1-Optimization of activated carbon preparation

In order to optimize the preparation of activated carbon, the Box-Behnken plan (PBB) was used. The experimental area of this study is given by the following table:

a) -Experimental area

Table 1: Experimental design

Natural variables	Encoded variables	Units	Levels		
			-1	0	+1
Ratio	A	G	1	1,5	2
Carbonization temperature	B	°C	300	400	500
Residence time	C	Min	60	90	120

This experimental design matrix leads us to an experimental matrix. The Box-Behnken design of experiment (PBB) giving the different level combinations of the variables (coded or not) is given by the Table. This design was generated by Minitab 16 software (Minitab 16 Inc., USA) and includes 15 experiments, the last three of which are the experiments at the center of the field of study whose purpose is to verify the reproducibility of the experiments. The experiments were conducted randomly to minimize systematic errors.

b) -Design of experiment and experimental conditions

Table 2: Experimental condition design

		Encoded variables			Real variables		
N° Exp	Blocs	A	B	C	Temperature	Time	Ratio
1	1	-	-	0	300	1,0	1,5
2	1	+	-	0	500	1,0	1,5
3	1	-	+	0	300	2,0	1,5
4	1	+	+	0	500	2,0	1,5
5	1	-	0	-	300	1,5	1,0
6	1	+	0	-	500	1,5	1,0
7	1	-	0	+	300	1,5	2,0
8	1	+	0	+	500	1,5	2,0
9	1	0	-	-	400	1,0	1,0

10	1	0	+	-	400	2,0	1,0
11	1	0	-	+	400	1,0	2,0
12	1	0	+	+	400	2,0	2,0
13	1	0	0	0	400	1,5	1,5
14	1	0	0	0	400	1,5	1,5
15	1	0	0	0	400	1,5	1,5

The results of experiments were compiled and subjected to an analysis of variance in order to verify the validation of the experimental model chosen; this again using Minitab 16 software.

In order to obtain activated carbons with interesting characteristics such as:

- A large specific surface area

- A developed micro and mesoporosity

- And high efficiency

We chose iodine number, methylene blue number and ACP yield as answers. These responses are recorded in the following table:

c)-Experimental responses studied

Table 3: Experimental reponses studied

	Reponses	Units
Iodine number	Y_1	$mg.g^{-1}$
Methylene blue number	Y_2	$mg.g^{-1}$
Yield	Y_3	%

II.3-Characterization of the adsorbent

II.3.1-Fourier Transform Infrared Analysis (IRFT)

The IRFT makes it possible to identify different chemical bonds and groups that are found on the surface of activated carbon. The principle is based on the irradiation of a sample by infrared radiation. The recorded signal represents the sum of the fringe intensities for each frequency, resulting in a curve called an interferogram. The absorption spectrogram is derived from the interferogram using the Fourrier transform **(Lekene, 2019)**. The absorption spectra were carried out in the mid-infrared range (400 cm^{-1} and 4000 cm^{-1}). The spectra of the materials were made at the Laboratory of Analytical Chemistry of the Faculty of Sciences of the University of Yaoundé I.

II.3.2-Differential and thermogravimetric thermal analysis (ATD/GTA)

The ATD and ATG were carried out at the University of Yaoundé I, Laboratory of Materials Chemistry. It makes it possible to determine and explain the different mass losses depending on the temperature that the material has undergone during heat treatment.

II.3.3-pH of zero charge point

Zero charge point pH (pHPCN) defines the pH at which the total number of positive and negative charges on the surface of a solid material is zero. Determining the pHPCN consists in preparing a NaCl solution of concentration 0.1 M at pH ranging between 2 and 10 by adding

NaOH or HCl. A volume V = 40 mL of each of the 0.1 M solutions is introduced into an Erlenmeyer containing 0.1 g of activated carbon. The determination of this point makes it possible to predict possible interactions between the molecules of the adsorbent and those of the adsorbate.

II.3.4-Scanning Electron microscopy

The scanning electron microscopy (SEM) is used to study the morphology and surface characteristics of adsorbent material.

II.4-Preparation of adsorbates

II.4.1-Indigo carmine

A stock solution (S_0) of concentration 1000 ppm is prepared by weighing 1.25 g of IC powder that has been introduced into a 1000 mL volumetric flask filled to 3/4 of the distilled water. The solution obtained is homogenized for 1 hour and then supplemented with distilled water to the gauge. Dilutes solutions of 1, 2, 3, 4, 5, 6, 7, 9, 10 ppm are obtained by successive dilutions of the stock solution in 100 mL volumetric flasks. These solutions will therefore be measured by UV-visible spectrophotometry at the wavelength of 610 nm. The calibration curve, $A = f(C_0)$, is then obtained by plotting the absorbance (A), as a function of the initial concentration C_0.

II.4.2-Copper (II) ion

A stock solution (So) of concentration 4000 ppm is prepared, weighing a mass of 16g of $CuSO_4.5H_2O$ that has been introduced into a 1000mL volumetric flask filled 3/4 with distilled water. The mixture will be stirred for 24 hours until completely dissolved. The solution obtained will be supplemented with distilled water up to the mark. Dilutes solutions of 100 to 1000 ppm will be obtained by successive dilutions of the stock solution in 100 mL volumetric flask. These solutions will therefore be measured by UV-visible spectrophotometry at the wavelength of 804 nm. The calibration curve, $A = f(C_0)$, is then obtained by plotting the absorbance (A), as a function of the initial concentration C_0.

II.5-Adsorption in batch mode

The adsorption of copper(II) ions and indigo carmine were carried out at room temperature, by taking 20 mL of each solution (copper(II) ions and indigo carmine) to which a mass of 0.02 g of material was added. After a stirring time, the mixtures are filtered using a Whatman filter paper and the filtrates obtained are assayed with a UV-visible spectrophotometer at a maximum wavelength of 804 nm and 610 nm respectively for copper(II) ions and indigo carmine. The amount adsorbed per unit mass of adsorbent (*Qe*) at equilibrium is given by

$$\boldsymbol{Qe} = \frac{(\mathbf{C_O} - \mathbf{C_t})\mathbf{x}\,\mathbf{V}}{\mathbf{m_{ACP}}}$$

Where C_o is the initial concentration of the adsorbate (mg/L), C_t is the equilibrium concentration of the adsorbate (mg/L), V is the volume of the solution containing the adsorbate (mL) and m is the mass of the adsorbent (g). The parameters we varied in this study are: the initial pH and the initial concentration of the adsorbate in solution. The stirring speed is kept constant throughout the experiment. The initial pH of the solutions was adjusted using hydrochloric acid and sodium hydroxide solutions of normality 0.1 N. The pH of the solutions obtained was measured using a pH meter.

III-RESULTS AND DISCUSSIONS

III.1-Characterization of the adsorbent material

For the characterization of our adsorbent, several methods were used such as thermal analysis, IRFT, zero charge point pH, SEM.

III.1.1 Thermogravimetric analysis (ATG/ATD/DSC)

The thermal analysis of our raw material (cocoa pod) allowed us to obtain the following thermogram:

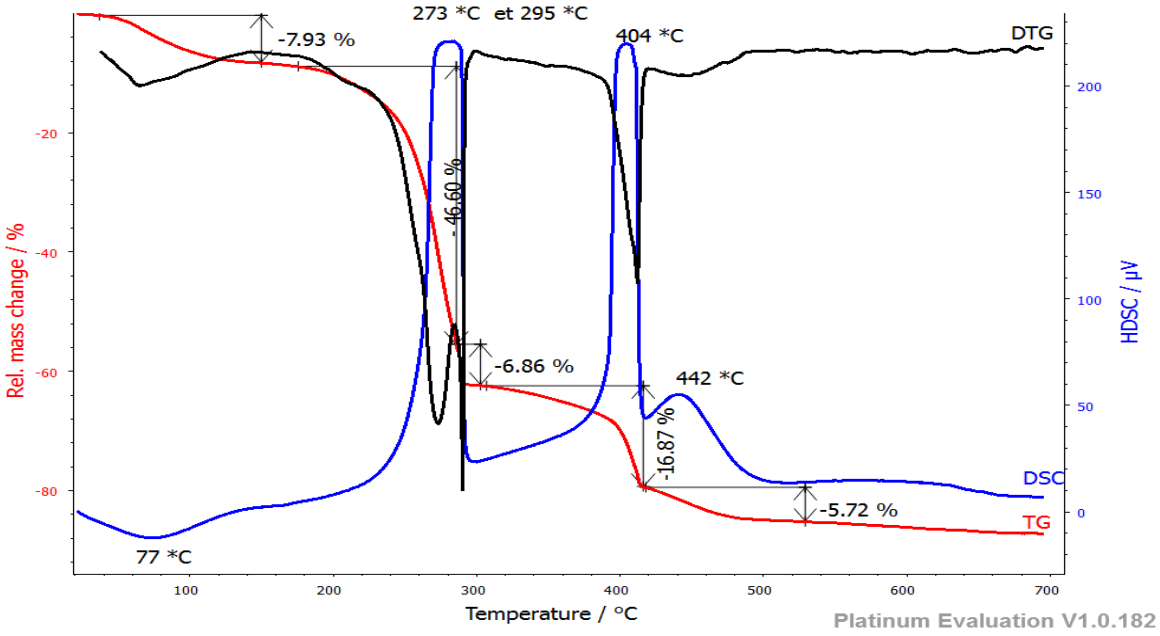

Figure 2: Cocoa pod thermogram TG-DSC

The figure 2 shows us the curve of TG and DSC. The TG curve reveals the different mass losses as a function of temperature, there are 5 mass losses and the DSC presents the exact temperatures at which they occurred:

Firstly, at 77 ° C, we observe an endothermic peak corresponding to a dehydration loss of water of the order of 7.93%; **(Lékéné et al., 2018)**. Secondarily, between 273 and 295, we observe an exothermic peak that could correspond to a decomposition of hemicellulose with a loss of mass of the order of 53.46%; **(Zhu et al., 2017)**. Thirdly, at 404 ° C, we observe an exothermic peak which could correspond to a decomposition of cellulose materialized by a loss of mass of 16.87%; **(Zhu et al.,2017)**. Fourtly, at 442 °C, we observe an exothermic peak that could correspond to the decomposition of lignin. This is materialized by a loss of mass of 5.72%; **(Lékéné et al., 2018)**.

From the ATG curve we can conclude that the best carbonization temperature is between 300 and 500°C because the temperature range corresponds to the decomposition of hemicellulose, cellulose and the main lignin constituting the carbon backbone of our biomass.

III.1.2-Fourier transform infrared spectroscopy of cocoa pods and ACP.

Infrared spectroscopy analysis identifies functional groups present on the surface of cocoa pods and on the surface of ACP. This analysis also provides information on the types of interactions involved during the adsorption phenomenon. The Figure 3 show respectively IR spectra of cocoa pods and the ACP obtained after phosphoric acid activation.

The IR analysis of our biomass presents us with the following results. At 3272 cm^{-1} there is the presence of the peak characterizing the presence of the stretching vibration of the -OH groups of alcohols, carboxylic acids and phenolic functions, 2929 cm^{-1} corresponds to the valence vibration bands are assigned to the C-H bond. Around 1728 cm^{-1} there is a band corresponding to the vibration frequency of C=O aldehydes, between 1369-1235 cm^{-1} bands corresponding to the C-O-C stretching frequency and at 1029 cm^{-1} the stretching vibration band could be attributed to aliphatic C-O bonds **(Ankoro et al., 2020)**.

The IR spectrum of the ACP shows us the absence of the characteristic peak of the OH group of alcohols and phenols, at 2920 cm^{-1} vibration frequency of the aliphatic C-H bond. The bands between 1705-1630 cm^{-1} correspond to the stretching frequencies of the C=O bonds, at 1161 cm^{-1} we have the frequency corresponding to the C-O bond of alcohols, 1070 cm^{-1} frequency of P-O or P=O **(Puziy et al., 2005)** and 990 cm^{-1} that of C-H deformation out of the plane.

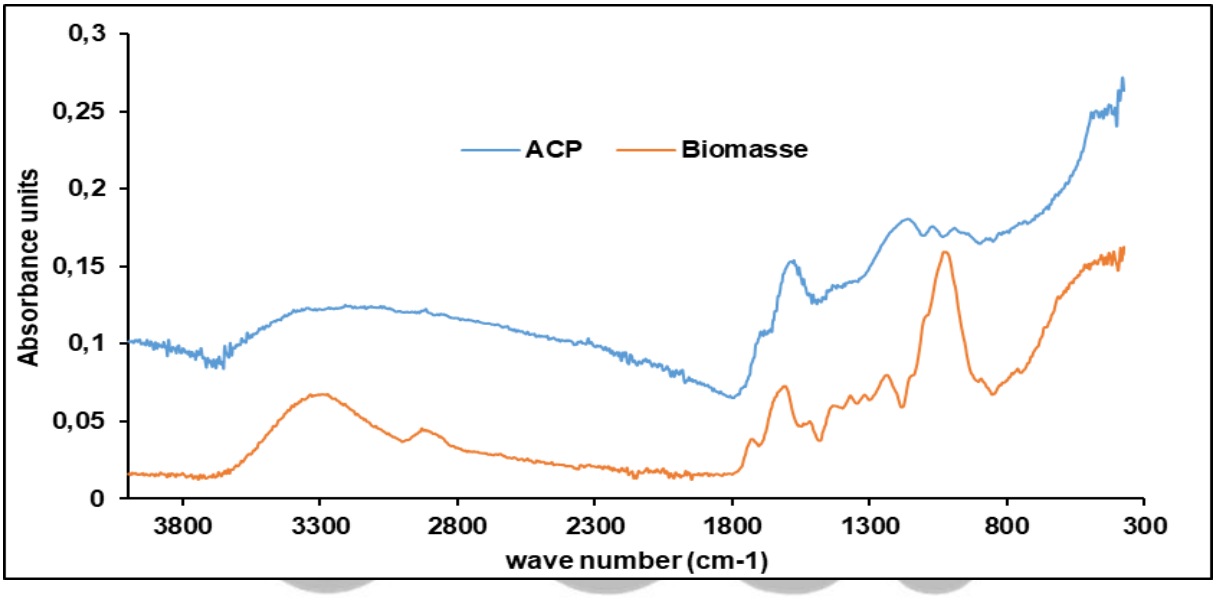

Figure 3: FTIR of cocoa pod and ACP

III.1.3-Textural study

- Nitrogen adsorption-desorption isotherms (BET-BJH).

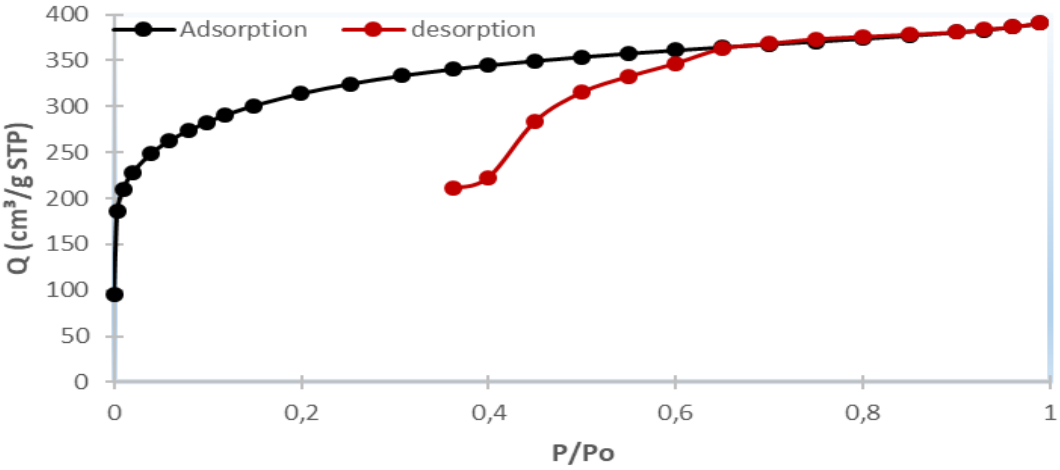

Figure 4a : Isotherme d'adsorption du CAP

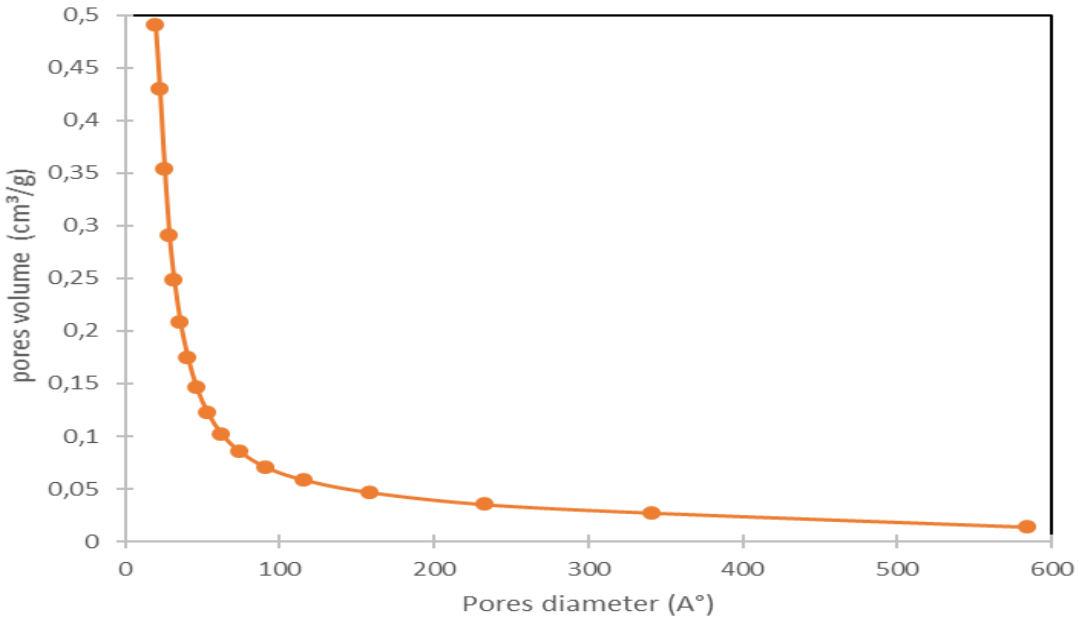

Figure 5b : Isotherme d'Adsorption Barret Joyner Halenda (BJH) et volume des pores dV/dD du CAP

- Scanning Electron Microscopy (SEM)

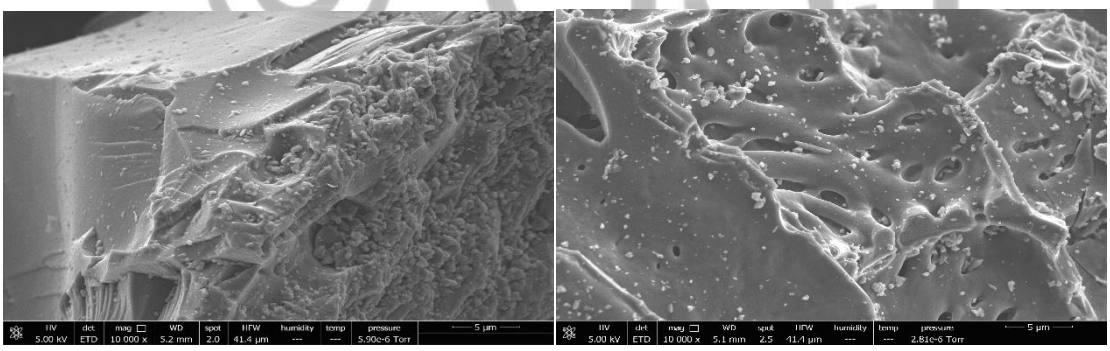

Figure 6c :SEM of ACP with 10000X magnitude

From figures 4c, we can see that there are pores on the ACP surface. The ACP surface is irregular, rough and highly porous indicating the possibility of its good adsorption properties. This can be explaining by the fact that activated agent play a mains role on the development of porosity.

III.2-Optimization of the preparation of H_3PO_4 activated carbon (ACP)

The table below lists the compilation of experimental values as well as the predicted values obtained after planning and modelling.

Table 4: Compilation of experimental and predicted values of ACP

Variables	**Y_1 (IN)**	**Y_2 (MBN)**	**Y_3 (Rdt)**

Exp n°	A T.°c	B Time	C Ratio	Exp	Pred	Exp	Pred	Exp	Pred
1	300	1,0	1,5	543,53	539,24	66,41	64,75	53,30	54,10
2	500	1,0	1,5	694,02	685,45	89,85	90,99	42,66	45,87
3	300	2,0	1,5	579,72	588,29	80,57	79,43	**60,00**	**56,79**
4	500	2,0	1,5	781,65	785,94	**89,85**	**91,51**	48,00	47,20
5	300	1,5	1,0	577,82	580,44	88,65	87,11	51,00	50,58
6	500	1,5	1,0	735,93	742,84	89,85	85,51	46,00	43,17
7	300	1,5	2,0	**480,66**	**473,76**	**46,98**	**51,32**	48,00	50,83
8	500	1,5	2,0	657,83	655,21	89,70	91,24	**40,00**	**40,42**
9	400	1,0	1,0	638,78	640,44	89,83	93,04	45,00	44,62
10	400	2,0	1,0	**785,46**	**774,27**	89,83	92,51	44,00	47,63
11	400	1,0	2,0	591,15	602,34	72,57	69,89	48,00	44,37
12	400	2,0	2,0	619,73	618,06	88,82	85,62	45,00	45,38
13	400	1,5	1,5	554,96	554,98	89,82	89,78	42,53	42,62
14	400	1,5	1,5	554,96	554,96	89,76	89,78	42,66	42,62
15	400	1,5	1,5	554,96	554,96	89,76	89,78	42,66	42,62

According to the table, it shows that the yield varies from 40 to 60%, the iodine value (IN) from 480.66 to 785.46 mg/g and the methylene blue value (IBM) from 46.98 to 89.85 mg/g. At the lowest temperature, maximum ratio and intermediate residence time we have the highest efficiency (experiment n°3) and its lowest value is obtained when the temperature is maximum, intermediate time and maximum ratio (experiment n°8). For iodine and methylene blue values are obtained in experiment 10 for IN and experiment 4 for IBM.

III.2.1-Optimization of linear regression coefficients

a) -Estimated regression coefficients for Yield (%R).

Terms	Coef	SE Coef	*T*	*P*
Constant	140,653	52,720	2,668	0,044**
Temperature (A)	-0,377	0,169	-2,232	0,076*
Time (B)	-38,010	28,937	-1,314	0,246
Ratio (C)	18,890	28,937	0,653	0,543
Temperature*Temperature	0,000	0,000	2,433	0,059*
Time*Time	15,247	7,501	2,033	0,098*
Ratio*Ratio	-3,713	7,501	-0,495	0,642
Temperature*Time	-0,007	0,036	-0,189	0,858
Temperature*Ratio	-0,015	0,036	-0,416	0,694
Time*Ratio	-2,000	7,206	-0,278	0,792

b) -Estimated regression coefficients for IN

Terms	Coef	SE Coef	*T*	*P*
Constant	1517,250	153,308	9,897	0,000**
Temperature (A)	-1,630	0,491	-3,322	0,021**
Time (B)	-693,910	84,150	-8,246	0,000**
Ratio (C)	-360,990	84,150	-4,290	0,008**
Temperature*Temperature	0,000	0,001	4,498	0,006**

Time*Time	280,990	21,812	12,883	0,000**
Ratio*Ratio	134,300	21,812	6,157	0,002**
Temperature*Time	0,260	0,105	2,455	0,058*
Temperature*Ratio	0,100	0,105	0,909	0,405
Time*Ratio	-118,110	20,956	-5,636	0,002*

c) -Estimated regression coefficients for MB

Terms	**Coef**	**SE Coef**	***T***	***P***
Constant	23,955	60,5238	0,396	0,709
Temperature (A)	0,4737	0,1938	2,444	0,058*
Time (B)	21,4025	33,2211	0,644	0,548
Ratio (C)	-78,0825	33,2211	-2,35	0,066*
Temperature*Temperature	-0,0007	0,0002	-3,386	0,02**
Time*Time	-3,285	8,6108	-0,381	0,719
Ratio*Ratio	-14,785	8,6108	-1,717	0,147
Temperature*Time	-0,0708	0,0414	-1,712	0,148
Temperature*Ratio	0,2076	0,0414	5,019	0,004**
Time*Ratio	16,25	8,273	1,964	0,107

The different Tables above present the results of the estimated linear regressions of %R, IN and MB.

For the case of the yield %R, we observe that among the linear terms only temperature has a significant effect with a P-value of 0.076, for the quadratic terms only time-time and temperature-temperature which have a significant effect (p-value 0.059 and 0.098) and no interaction term is significant. The estimated linear coefficients for the IN show all very significant linear terms with p-values of 0.000, 0.021 and 0.000; identical results for quadratic terms (P-value 0.008; 0.006 and 0.000). Only the term temperature-ratio interaction is not significant. With regard to the estimated regression coefficients of the MB, it follows that the significant linear terms are temperature and the ratio with P-values 0.058 and 0.066; the only very significant quadratic term is temperature-temperature with its P-value of 0.002 and the very significant interaction term (P-value 0.004) is temperature-ratio.

The results obtained allowed us to establish equations of the regression model.

III.2.2-Mathematical Modeling development of the regression model equation

The quadratic model was selected as suggested by Minitab 16 software for the response representation. The following equations represent the final empirical model formulas for diode index (Y_1), methylene blue number (Y_2) and yield (Y_3).

$$Y_1 = 140{,}653 - 0{,}377A - 38{,}010B + 18{,}890C + 15{,}247B^2 - 3{,}713C^2 - 0{,}007AB - 0{,}015AC - 2{,}000BC$$

$$Y_2 = 1517{,}250 - 1{,}630A - 693{,}910B - 360{,}990C + 280{,}990B^2 + 134{,}300C^2 + 0{,}260AB + 0{,}100AC - 118{,}110BC$$

$$Y_3 = 23{,}955 + 0{,}4737A + 21{,}4025B - 78{,}0825C - 0{,}0007A^2 - 3{,}285B^2 - 14{,}785C^2 - 0{,}0708AB + 0{,}2076AC + 16{,}250BC$$

The weight of the particular factor is represented by the one-factor coefficient while the weight of the interactions between two factors and the weight of the quadratic effect are represented respectively by the coefficients with two factors and those with second-order terms. The positive sign in front of a term indicates a synergistic effect while the negative sign indicates an antagonistic effect.

III.2.3-Results of the analysis of variance (ANOVA) for the ACP

The processing of model results is based on an analysis of variance. The results are compiled in the Tables: The confidence level is set at 95%. The mean squares value was obtained by dividing the sum of the squares of each source of variation by their respective degrees of freedom. A factor is said to be statistically significant when the value of F is high or the value of P is less than 0.05. When the P value is between 0.05 and 0.1, the factor is weakly or insignificant and not significant when greater than 0.1 **(Lékéné et al., 2018)**.

a) -Analyses of Variance of the %R

Table 5: Results of the %R Analyses of variance

Source	DF	Seq SS	Adj SS	Adj MS	*F*	*P*
Regression	9	303,711	303,711	33,746	2,600	0,153
Linear	3	169,981	95,978	31,993	2,460	0,177
Temperature (A)	1	158,776	64,652	64,652	4,980	0,076*
Time (B)	1	8,080	22,399	22,399	1,730	0,246
Ratio (C)	1	3,125	5,532	5,532	0,430	0,543
Square	3	130,017	130,017	43,339	3,340	0,114
Temperature*Temperature	1	70,830	76,833	76,833	5,920	0,059*
Time*Time	1	56,005	53,645	53,645	4,130	0,098*
Ratio*Ratio	1	3,182	3,182	3,182	0,250	0,642
Interaction	3	3,712	3,712	1,238	0,100	0,959
Temperature*Time	1	0,462	0,462	0,462	0,040	0,858
Temperature*Ratio	1	2,250	2,250	2,250	0,170	0,694
Time*Ratio	1	1,000	1,000	1,000	0,080	0,792
Residual Error	5	64,913	64,913	12,983		
Lack-of-Fit	3	64,901	64,901	21,634	3840,320	0,000**
Pure Error	2	0,011	0,011	0,006		
Total	14	368,623				

According to Table 5, the F and P values of the model describing the yield (%R) are 2.600 and 0.153 respectively, only the F-value makes the model significant because it is high. In view of the results obtained, we see that the terms linear, quadratic and interaction are all insignificant because their P-value is greater than 0.1. Despite this, the model has temperature (P-value = 0.076) as factors of the linear term not very significant, temperature-temperature (P-value =

0.059 and 0.098) as factors of the linear term not significant, and no factor of the term interactions is significant. Regarding the values of the "sum of squares", we note that they are very far from the values of the "adjusted sum of squares", which is in agreement with the results of the P-value; but despite this the P-value of the "Lack-of-fit" is very significant (0.000) which shows that the model can be accepted after further necessary verifications.

b) -Analyses of variance of the IN

Table 6: Results of analyses of variance of the IN

Source	DF	Seq SS	Adj SS	Adj MS	*F*	*P*
Regression	9	115677,000	115677,000	12853,000	117,070	0,000**
Linear	3	89176,000	8466,000	2822,100	25,710	0,002**
Temperature (A)	1	59116,000	1212,000	1211,800	11,040	0,021**
Time (B)	1	11181,000	7465,000	7465,400	68,000	0,000**
Ratio (C)	1	18878,000	2020,000	2020,400	18,400	0,008**
Square	3	22261,000	22261,000	7420,500	67,590	0,000**
Temperature*Temperature	1	1093,000	2221,000	2221,300	20,230	0,006**
Time*Time	1	17006,000	18220,000	18220,500	165,960	0,000**
Ratio*Ratio	1	4162,000	4162,000	4162,300	37,910	0,002**
Interaction	3	4240,000	4240,000	1413,200	12,870	0,009**
Temperature*Time	1	662,000	662,000	661,500	6,030	0,058*
Temperature*Ratio	1	91,000	91,000	90,700	0,830	0,405
Time*Ratio	1	3487,000	3487,000	3487,500	31,770	0,002**
Residual Error	5	549,000	549,000	109,800		
Lack-of-Fit	3	549,000	549,000	183,000	*	*
Pure Error	2	0,000	0,000	0,000		
Total	14	116226,000				

The value of F and P for this model describing the IN are 117.070 and 0.000 respectively shows the very significant model (Table 6). The values of the linear, quadratic and interaction terms (0,002,0,000 and 0,009) are very significant; moreover, all the factors of the linear term are very significant P-value<0.05 (temperature, time and ratio with P-values of 0.000,0,008 and 0.000), as well as those of the quadratic term (temperature-temperature, time-time and ratio-ratio with P-values of 0,006,0,000 and 0.002). Regarding the factors of the interaction term, time-ratio is very significant and temperature-time insignificant with P-values of 0.002 and 0.058; Only the term temperature-ratio is not significant. Looking at the results of the "sum of squares" and "adjusted sum of squares", we see that they are very close and in agreement with the results of the P-values which makes the model reliable and significant.

c)-MB Analyses of Variance

Table 7: Results of MB Analyses of variance

Source	DF	Seq SS	Adj SS	Adj MS	*F*	*P*
Regression	9	2080,960	2080,960	231,218	13,510	0,005**
Linear	3	1301,160	255,290	85,097	4,970	0,058*
Temperature (A)	1	734,210	102,190	102,190	5,970	0,058*
Time (B)	1	115,600	7,100	7,102	0,420	0,548
Ratio (C)	1	451,350	94,530	94,525	5,520	0,066*
Square	3	232,680	232,680	77,560	4,530	0,069*
Temperature*Temperature	1	181,160	196,160	196,157	11,460	0,020**
Time*Time	1	1,070	2,490	2,490	0,150	0,719
Ratio*Ratio	1	50,450	50,450	50,445	2,950	0,147
Interaction	3	547,120	547,120	182,373	10,660	0,013**
Température*Time	1	50,130	50,130	50,126	2,930	0,148
Temperature*Ratio	1	430,980	430,980	430,978	25,190	0,004**
Time*Ratio	1	66,020	66,020	66,016	3,860	0,107
Residual Error	5	85,550	85,550	17,111		
Lack-of-Fit	3	85,550	85,550	28,517	23764,260	0,000**
Pure Error	2	0,000	0,000	0,001		
Total	14	2166,510				

The table 7 shows us the F and P-value for this model describing the MB are 13.510 and 0.005 respectively shows the significant model. The P-values of the linear, quadratic and interaction terms (0.058, 0.069 and 0.013) show the significant model because it is between 0 and 0.1. The factors of the linear term not very significant are temperature and time (P-value of 0.058 and 0.066), a single factor of the quadratic term (temperature-temperature) and the interaction term (temperature-ratio) are very significant with P-values of 0.020 and 0.004 and the rest not significant because of their high P-value. Moreover, with regard to the values of "sum of squares" and "adjusted sum of squares" of the terms quadratic and interaction which are perfectly identical, this model can perhaps be considered reliable and valid. This result is in line with the P-value of "Lack-of-fit" (0.000) which is very significant.

Réponse	R^2	R^2 (pred)	R^2(adj)
%R	82,39%	0 ,00%	50,69%
IN [Quantité adsorbée (Q_e)/mg/g]	99,53%	92,44%	98,68%
BM [Quantité adsorbée (Q_e)/mg/g]	96,05%	36,82%	88,94%

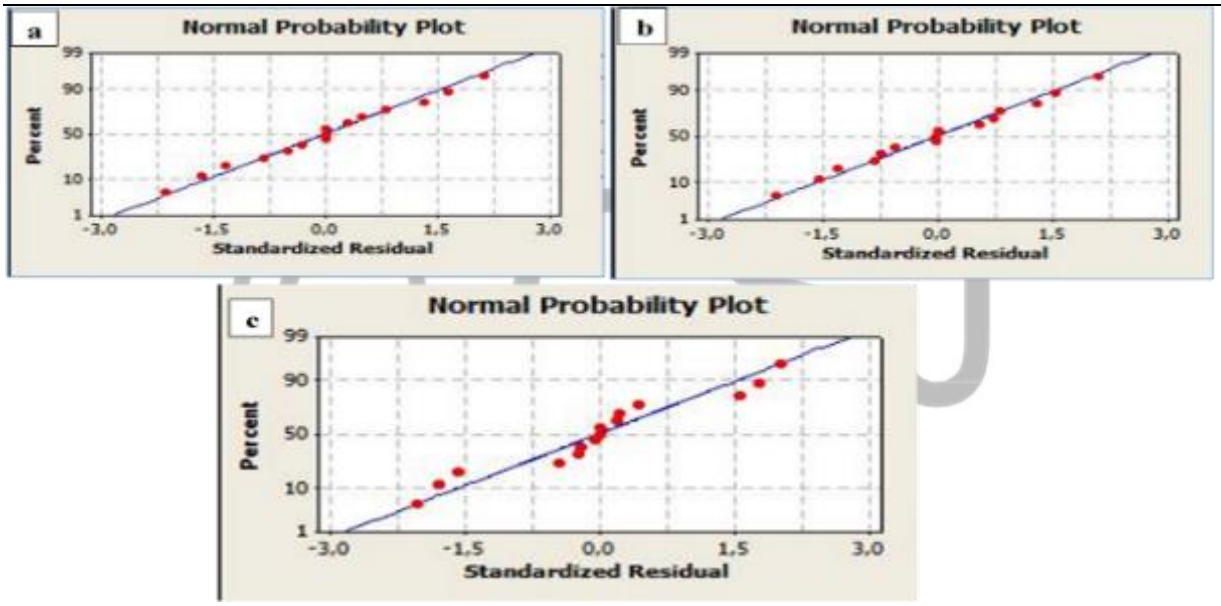

Figure 7: Normal probability plot a) yield, b)IN and c) MBN

The normal probability plot versus residuals were plotted to verify the validity and reliability of the models against ANOVA's assumptions. The data is said to be normally distributed if the points are very close to the right. Regarding our results, the figure 4 shows us that the points are quite close to the line from which we can conclude that our model is reliable.

III.2.4-Values of correlation coefficients

Table 8: Value of correlation coefficients

Table 8 shows the values of R^2 for equations tree equations are 82.39%, 99.53% and 96.05% of the total variation in %R, IN and MB were explained by this model. It also shows from the

Table that the model could not explain 17.71%, 0.47% and 3.95% of the independent variables of the %R, IN and MB responses relating to independent reactions. Similarly, we note the values of R^2 and adjusted R^2 of IN and MB are greater than 0.8 at a confidence level of 95%, which implies that the models developed for these two answers better explain the results obtained. Despite this, the adjusted R^2 value of R% is less than 0.8 and is therefore considered moderate for this model. These results are consistent with those obtained previously.

a-Determination of iodine number

The ANOVA results showed us that all the factors studied (time, temperature and ratio) are significant given their low P values (<0.05). The following figures show respectively the contour plot (2-dimensions) and the response surface (3-dimensions) obtained when plotting IN as a function of the ratio, time and temperature when time is kept constant.

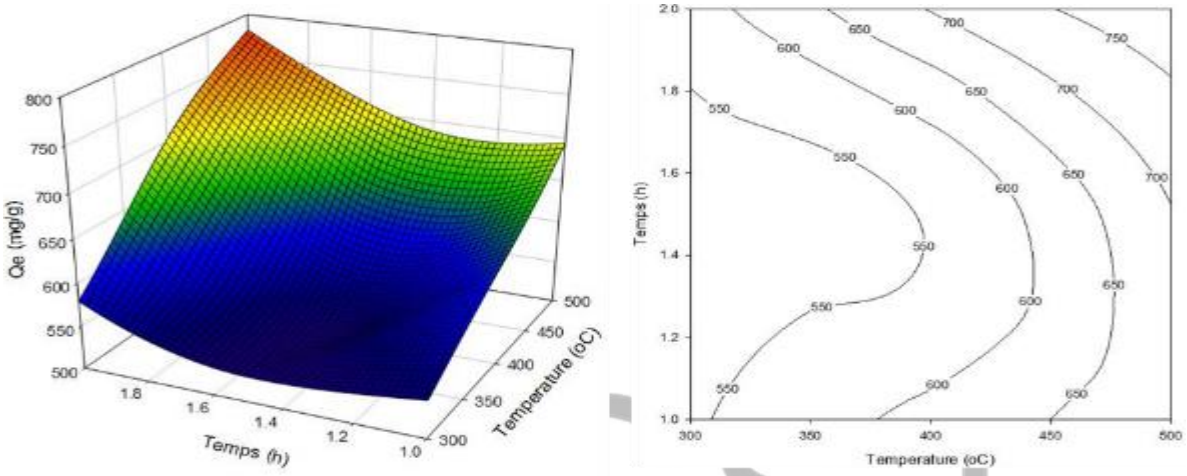

Figure 8: Response surface and contour plot of IN: Time-Temperature effect

The figure 6 shows the evolution of the iodine value as a function of time and temperature. We observe that the IN increases with temperature and carbonization time, this may be due to the fact that the increase in temperature favors the removal of volatile matter contained in the raw material and leads to the creation of new pores **Lekene et al 2018**.

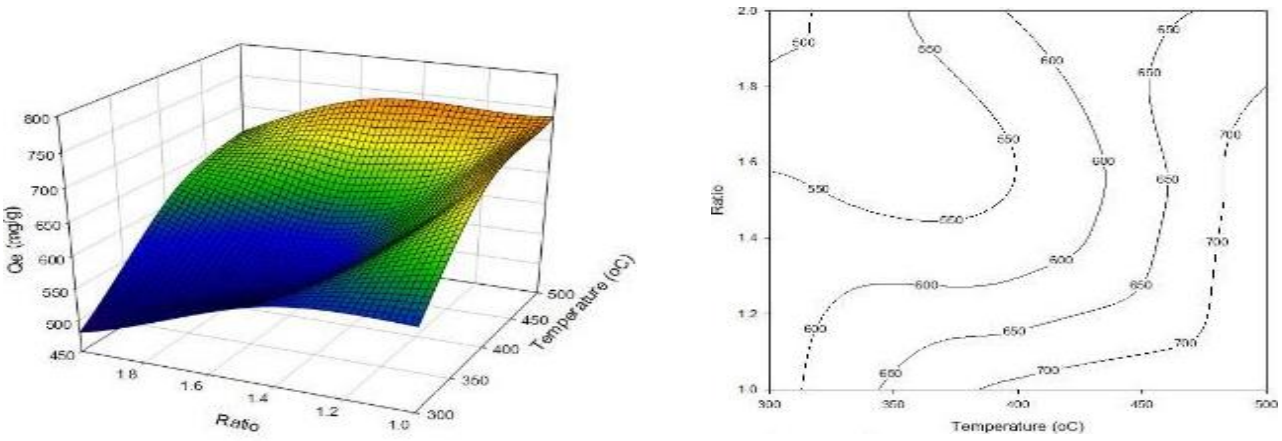

Figure 9: Response surface and contour plot of IN : Ratio-Temperature effect

The figure 7 shows the influence of ratio and temperature on IN. From this we notice that the IN decreases with the increase in the ratio, this may be due to: the formation of phosphates during pyrolysis and which would be clogging the pores or the dehydration of micropores in

larger pores caused by the excess of H_3PO_4 which disfavors the adsorption of I_2 **Lekene et al 2018.**

b) -Determination of methylene blue number

According to ANOVA, only temperature and ratio are the significant factors ($p<0.05$). The following figures show the plots of the contour curve (2-dimension) and the response surface (3-dimension) obtained by the analysis of the interaction between the ratio and the temperature identified by ANOVA as significant factors on the BM index when time is kept constant

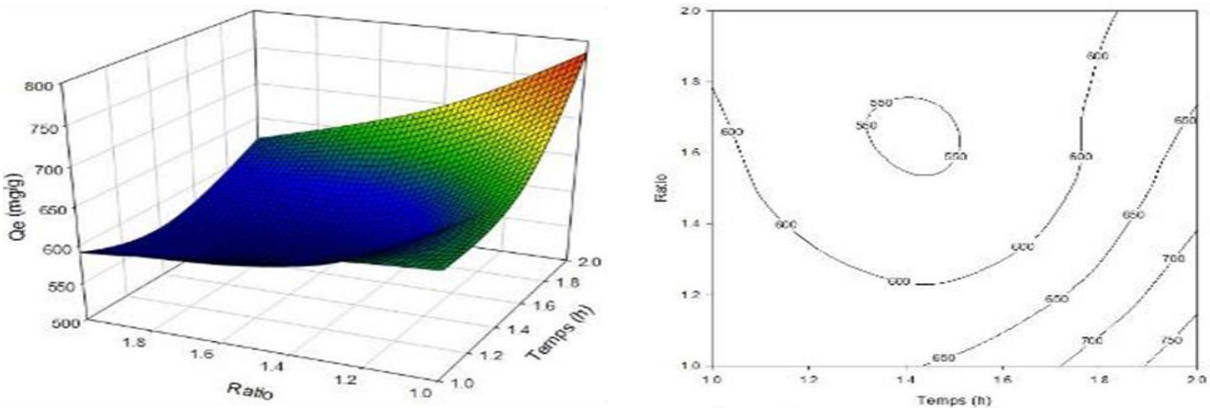

Figure 10: Response surface and contour plot of MB : Time-Ratio effect

From the figure 8, it emerges that the BM index grows proportionally with the increase in temperature and the ratio. This may be due to the depolymerization of cellulose releasing more mesopores, the increase in temperature leads to the opening and widening of pores favoring the adsorption of large molecules such as BM. These results are in agreement with those of **Kouotou et al (2013) and Lékéné et al (2018).**

c)-Yield

For the yield the ANOVA showed temperature and time as significant on the response, this because of the value of $P<0.05$. These two factors were used for the plotting of the contour curve (2-dimension) and the response surface (3-dimension).

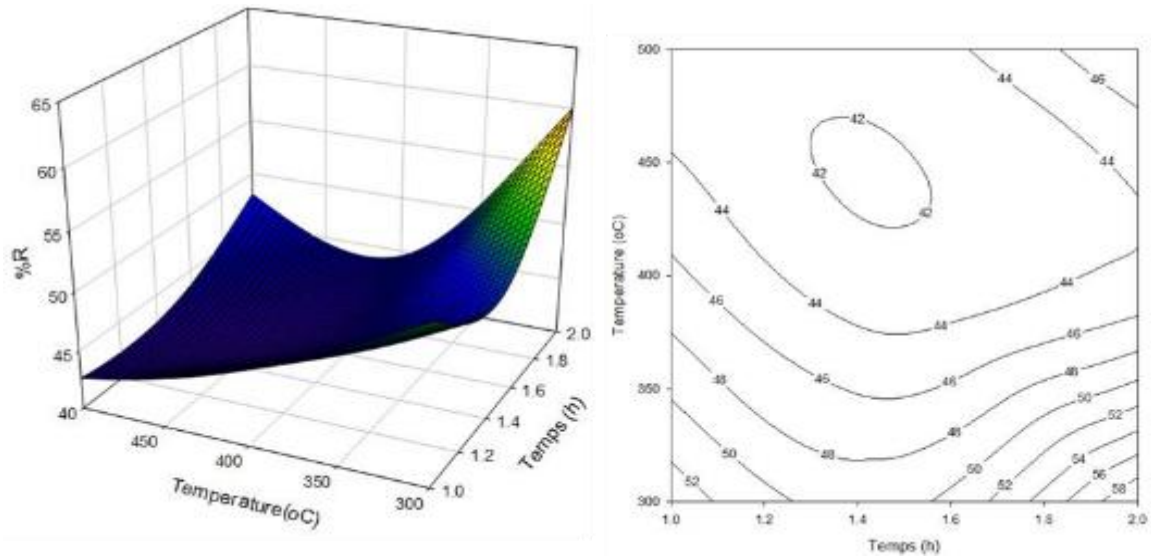

Figure 11: Response surface and contour plot of Yield :Time-Temperature effect

From figure 9 we can see that when the temperature increases, the activated carbon yield decreases. The carbonization time has a less significant effect on yield. High yield values are

obtained when the temperature and residence time are at their smallest values. These results are in agreement with those of **Lékéné et al (2018**) on pistachio shells and those of **Ahmed et al (2010)** on rattan sawdust who all found that the carbonization temperature has a very important role on the yield unlike the residence time which has a lesser effect. These results were predictable because carbonization produces volatile materials (CO_2, CO, H_2O, CH_4 ... etc.) which come from the degradation of cocoa pods at high temperature hence the low yield. This decrease can also be attributed to the thermal degradation of phospho-carbon species obtained after impregnation of the precursor with phosphoric acid and reduction of phosphates to elemental phosphorus (P_4O_{10}).

III.3-Determination of the zero-point charge

The pHPCN is the pH value at which the net surface charge is zero. In other words, it indicates the acidic or basic character of the surface of the adsorbent. In aqueous solution, the exchanges between the functions of the surfaces of the adsorbents and those of the adsorbate require knowledge of the zero charge point of the materials highlighted. The representation $pH_f = f(\Delta pH)$ of the Figure below whose intersection of the curves with the first bisector gives the zero charge point of the materials

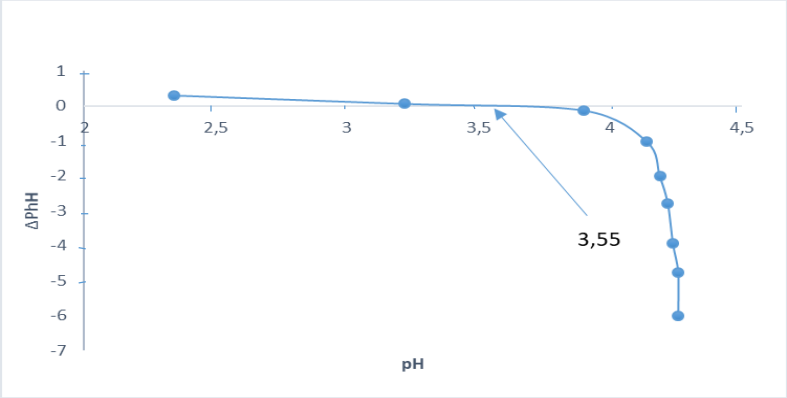

Figure 12: Zero charge point pH of ACP

In solutions whose pH values are lower than the pH of the zero point of load, the surface of the coals will be positively charged and if not, it will be negatively charged. In other words, when the pH of the solution is lower than the pHPCN of the material, the adsorption is favorable for an anionic analyte. Otherwise, it is favorable for a cationic analyte **(Maazou et al., 2017).** In the case of our study, it is generally noted that activated carbon has a pH below 7, which shows that acidic functional groups dominate on its surface.

III.4-Experiments Adsorption in batch mode

In order to know the favorable conditions for the adsorption of indigo carmine and copper (II) ions in aqueous solution, parameters such as the pH of the solution, the contact time, the mass of activated carbon, the concentration of adsorbate in solution were studied

III.4.1Influence of pH

a) -IC solution

This study was carried out with a solution of IC of 80ppm, a volume of 20mL, a mass of ACP m = 0.02g for a time t = 25min at pH ranging from 2 to 10 and the results obtained are presented by the graph (*Qe = f (pH)*) of the Figure 11:

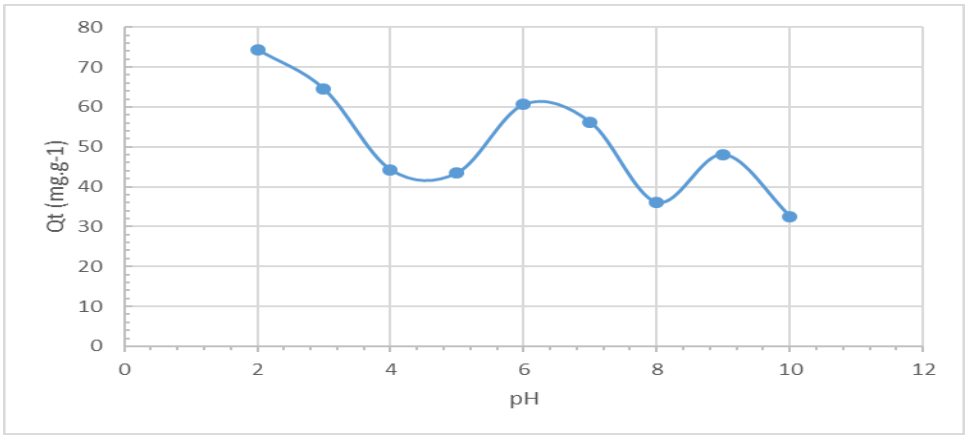

Figure 13: Influence of pH on IC adsorption

According to figure 10, the maximum adsorption of indigo carmine is observed at pH = 2 with adsorbed amount *Qe* = 74.4 mg / g. This result could also be explained by the fact that at pH = 2, the functional groups present on the surface of this material undergo a strong protonation **(Ndifor et al., 2017)**. This results in a strong electrostatic attraction between the positively charged functional groups on the surface of the adsorbents and the molecules of the IC. Thus at this pH, adsorption seems to be electrostatic in nature. Adsorption decreases significantly as pH increases. This is because the attractive forces become weaker probably by gradually decreasing the positive charge of the surface of the coal. Indeed, when the pH of the solution increases, the number of negatively charged sites increases. These results are in agreement with the results of pHPCN because at low pH (pH<pHpCN) the overall surface charge of the CAP is positive because the functional groups of the surface of the adsorbent are protonated which increases the electrostatic attraction between the positively charged CAP sites and the negatively charged dye, the adsorbent will become attractor. At pH=2, there is almost no electrostatic repulsion between the ACP and the dye, so the amount adsorbed is at its maximum **(Ngaha et al., 2019)**. These results are consistent with the work done by **Ndifor et al.,2017 and Ankoro et al.,2019.**

b) -Copper (II) solution

This study was carried out with a Cu^{2+} ion solution of 1000 ppm, a volume of 20 mL, a mass of CAP of 0,02 g for a time of 30min at pH ranging from 3 to 5.5, and the results obtained are given by the graph Qe = *f (pH)* of the following Figure:

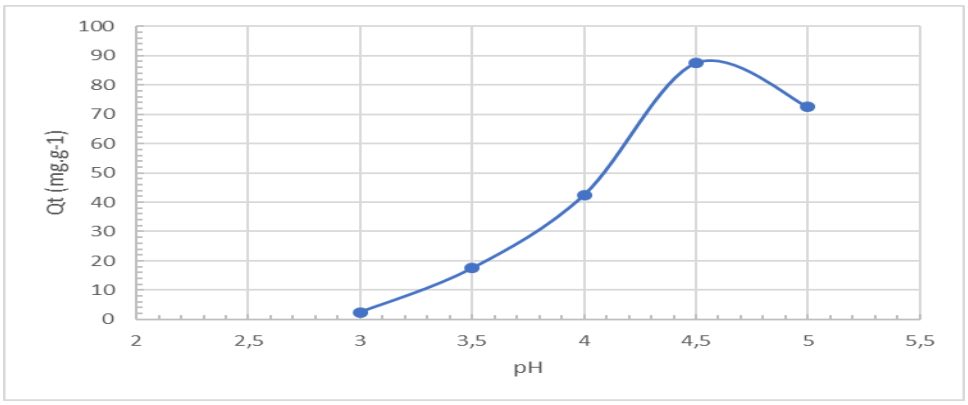

Figure 14: Influence of pH on Cu(II) ions adsorption

The curve obtained clearly shows that the amount adsorbed is considerably affected by the initial pH of the solution. Indeed, the adsorbed amount increases with pH up to 4.5 for Cu(II) ions with an adsorbed amount of 87.5 mg/g. The low adsorption at pH = 3 can be explained by

the fact that at this pH, there is competition between H^+ ions and Cu(II) ions, moreover the mobility of H^+ ions is higher than that of Cu(II) ions. Thus the surface of the material is positively charged because surrounded by H^+ ions. On the other hand, the higher the pH, the more there is therefore a decrease in the competitive effect between H^+ ions and Cu(II) ions, consequently increasing the amount of adsorption of Cu(II) ions **(Abéga et al., 2015)**. Beyond this pH, there is precipitation of Cu(II) ions.

III.4.2-Influence of adsorbate concentration

a) -IC solution

The influence of the initial concentration was studied by varying the IC concentration from 50 to 100 mg/L for 40 minutes with a 0.02 g ACP all at pH = 2. The curve in Figure 13 has been obtained.

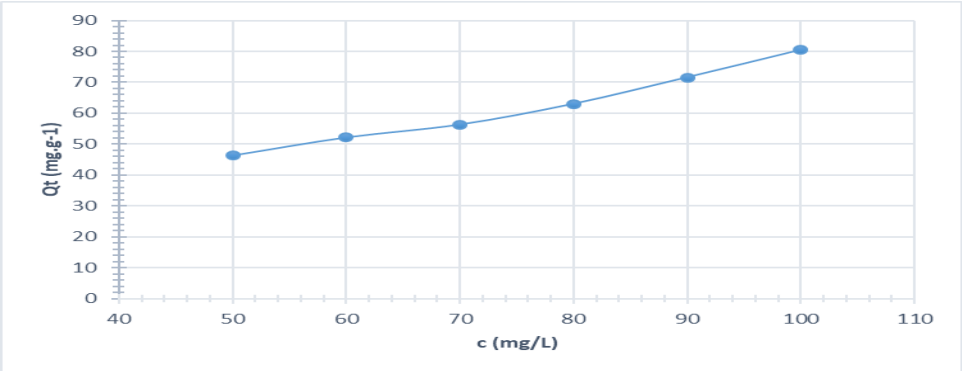

Figure 15: Influence of concentration on IC adsorption

We find that (figure 12), the amount of IC removal increases as its concentration increases. This could be explained by the fact that the increase in concentration leads to a decrease in the distance between the molecules of the adsorbate, leading to an increase in collisions between adsorbents and adsorbate hence an increase in the number of ions in solution that will diffuse towards the surface of the sites of the particles of the carbons and consequently the retention becomes more important. This may be because of the increase of the concentration gradient between the bulk solution and solid-liquid interface at high initial concentrations which results in an increase in the amount of adsorbed IC **(Abo El Naga et al.,2019).**

b) -Copper (II) solution

The influence of the initial concentration was studied by varying the IC concentration from 600 to 1600 mg/L for 35 minutes with a 0.02 g ACP all at pH 3.5. The curve of the Figure 14 has been obtained.

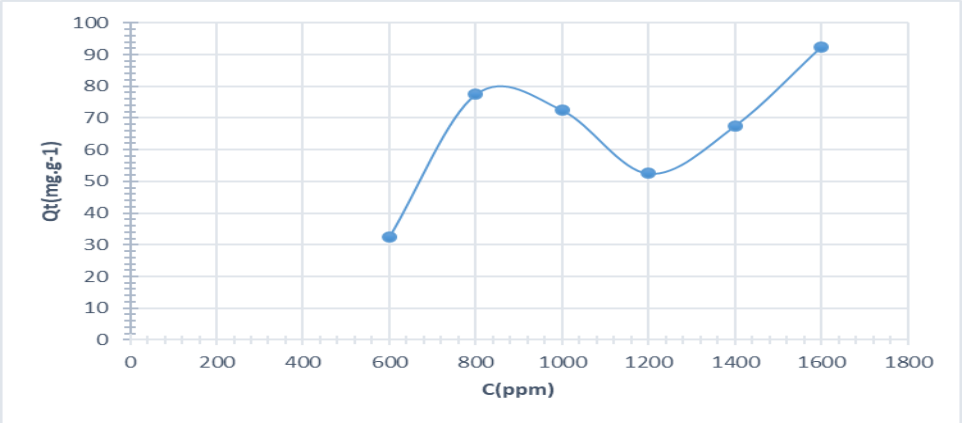

Figure 16: Influence of concentration on Cu(II) ions adsorption

According to Figure 13, when the concentration ranges from 600 to 800 there is an increase in the amount adsorbed. This was attributed to increased carbon surface area and the availability of more adsorption sites **(Arivoli et al., 2009)**. This increase in the amount adsorbed with the initial concentration is due to the fact that the increase in the initial concentration of copper ions leads to an increase in the occupation of adsorption sites; This intensifies the adsorption process. Beyond 800ppm (from 800 to 1000 ppm), we observe a decrease in the amount adsorbed from respectively 152.5 mg/g to 117.5 mg/g this is explained by the fact that, at very large concentrations, there is accumulation of copper molecules on the surface of our ACP which results in a reduction in the diffusion path of copper ions to adsorption sites. Moreover, from 1200 to 1600 ppm, the amount adsorbed still increases considerably, this could be explained by a phenomenon of continuous adsorption during which there is simultaneous adsorption with creation of new adsorption sites as the concentration increases **(Mohammed Jaafar et al.,2019)**. This evolution is characterized by diffusion in the mesopores and subsequently in the micropores.

Table 9: Comparative table of adsorption capacities of IC and Cu(II) ions

Adsorbents	Adsorbates	Qe(mg/g)	Références
Activated Carbon Based *Ricinodendron Heudelotti* Shells	IC	133,47	Ankoro *et al.*,2020
Pistia stratiotes dry biomass	IC	41,2	Rachel *et al.*,2019
Palm oil fiber	IC	128 ,44	Ngaha *et al.*,2019
Carbonaceous material	IC	92,83	Guti´errez-Segura *et al.*,2009
Brazil nut shells	IC	1,09	S. De Oliveira *et al.*,2010
Cocoa pod with H_3PO_4	IC	80,42	Present study
Cashew nut shell	Cu(II)	20 ,00	P.SenthilKumar *et al.*,2010
Rice shell	Cu(II)	1,85	H. Aydin *et al.*,2010
Peanuts hull	Cu(II)	21,25	S. Zhu et al.,2010
Cinnamomum camphora leaves powder	Cu(II)	16,76	H. Chen *et al.*,2010
Cocoa pod with H_3PO_4	Cu(II)	167,5	Present study

III.5-IR spectrum of CA-H_3PO_4 after adsorption of Cu^{2+} and IC

The Figures 14 and 15 shows the IR spectra before and after adsorption of IC and Cu^{2+} ACP ions. Note that these spectra are almost identical. On the IR spectra of ACP after adsorption of IC and Cu^{2+}, there is a decrease in the intensity of all peaks and the disappearance of some peaks

including the one located at 1070 cm^{-1}. This difference could be due to the adsorption of pollutants and it suggest the participation of the functional group in adsorption of Indigo-carmine by ACP.

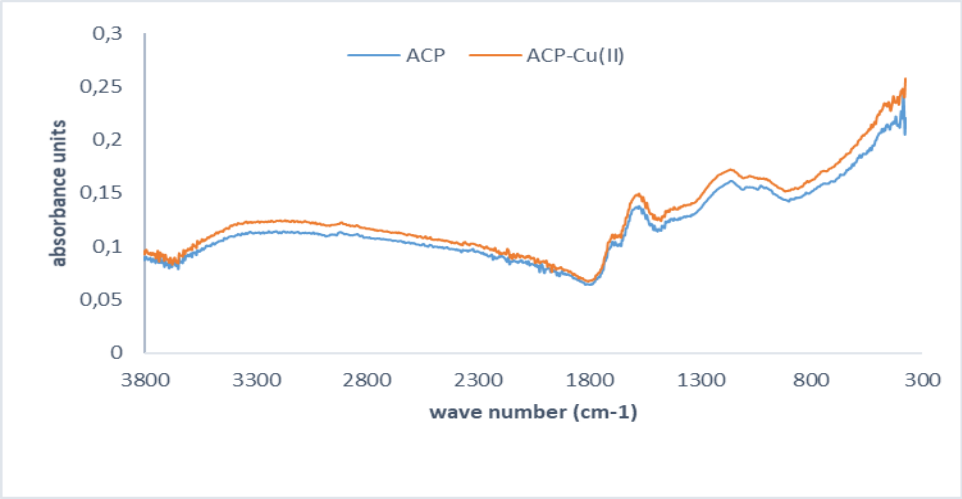

Figure 17: FTIR spectrum before and after adsorption of Cu(II) ions

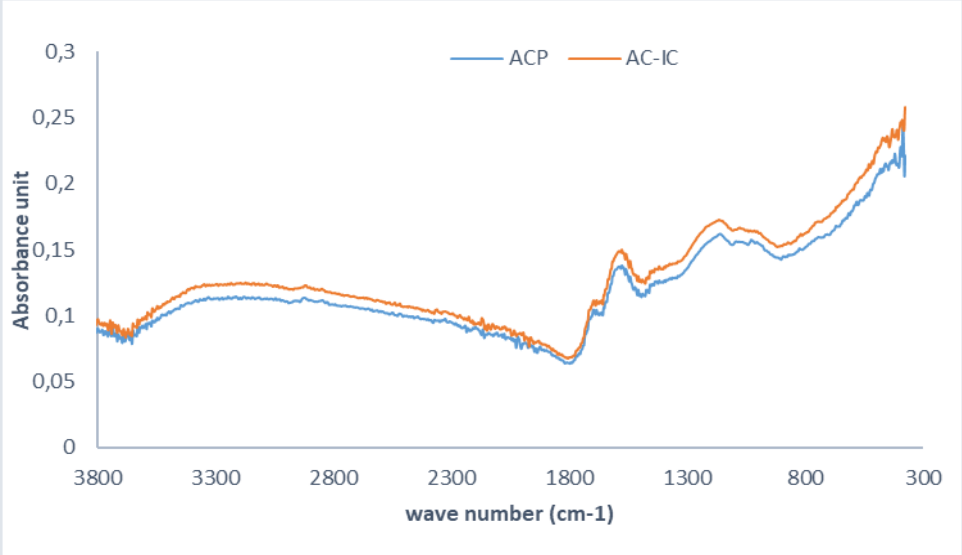

Figure 18: FTIR spectrum before and after adsorption of IC

III.6-Isothermal models

Adsorption isotherms play an important role in determining maximum adsorption capacities and in identifying the type of adsorption to occur.

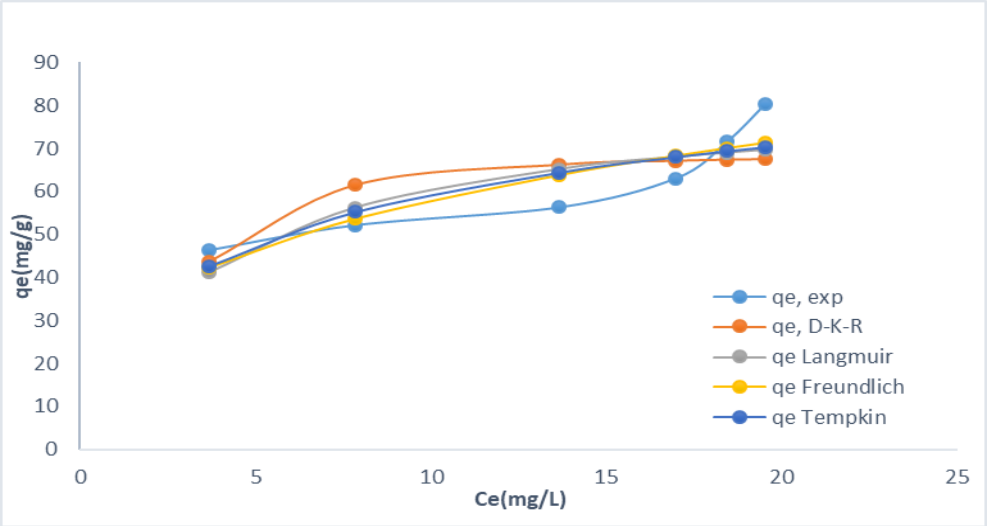

Figure 19: Non-linear isotherm for IC adsorption

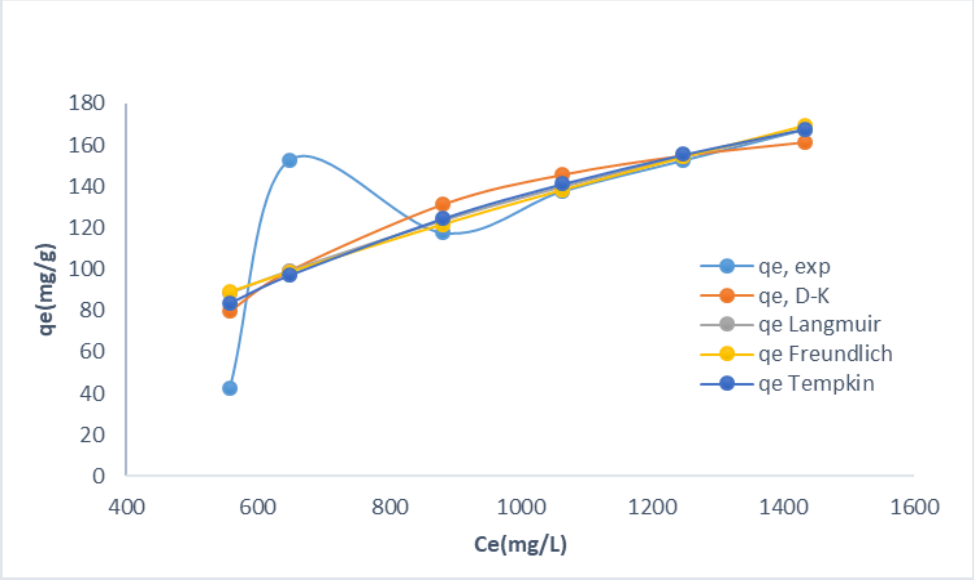

Figure 20: Non-linear isotherm for Cu(II) ions adsorption

Table 10: Non-linear isotherm parameters of IC and Cu(II) ions adsorption by ACP

Models	**Parameters**	**ADSORBATES**	
		IC	**Cu(II)**
Langmuir	$\mathbf{R^2}$	0,666	0,512
	$\mathbf{Q_m}$ **(mg /g)(théo)**	82,890	390,078
	$\mathbf{K_L}$ **(L/mg)**	0,269	0,001
	RMSE	8,204	35,391
	$\chi\mathbf{2}$	4,278	4238,457
Freundlich	$\mathbf{R^2}$	0,768	0,504

	K_F(mg /g)(L/mg)$^{-1/n}$	28,145	1,198
	1/n	0,313	0,681
	RMSE	6,830	35,694
	χ2	2,896	53,988
	R^2	0,718	0,528
	K_L (L/mg)	3,503	0,005
Tempkin	**b_T (KJ/mol)**	3149,205	28,041
	RMSE	7,541	34,810
	χ2	3,497	52,500
	R^2	0,512	0,556
	K_{DKR}	1,27E^{-6}	0,042
DKR	**Q_m**	68,812	183,013
	RMSE	6,038	48,589
	χ2	9,910	33,746
	E	5,04E^{-4}	0,059

The K_l value of Langmuir and 1/n of Freundlich between 0-1 shows the adsorption favorable for the 2 adsorbates, the values of E <8kj which means that there is competition between chemisorption and physisorption, in view of the values of R^2, none of the models was not suitable to represent the equilibrium adsorption data due to its lowest values of R^2 and very high values of RMSE and χ2

III.7-Study of adsorption kinetics

Adsorption kinetics is very important because it makes it possible to determine the efficiency of adsorption through the determination of the pollutant removal rate and the time required to reach equilibrium and also to predict the limiting steps of the process **(Ankoro et al, 2020)**. Four models were chosen to evaluate this: Pseudo-First Order, Pseudo-Second Order, Elovich and Intra-Particle Diffusion.

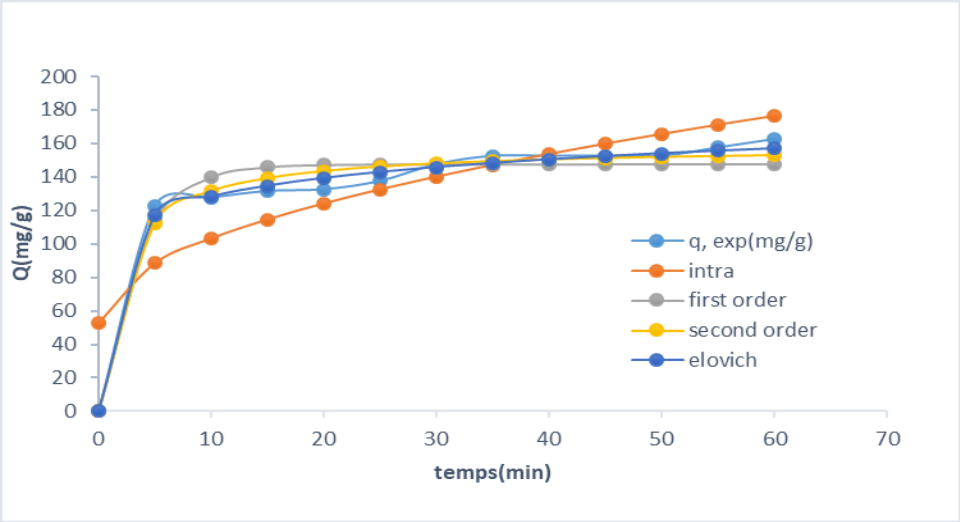

Figure 21: Non-linear representation of kinetic model for Cu(II) ions adsorption

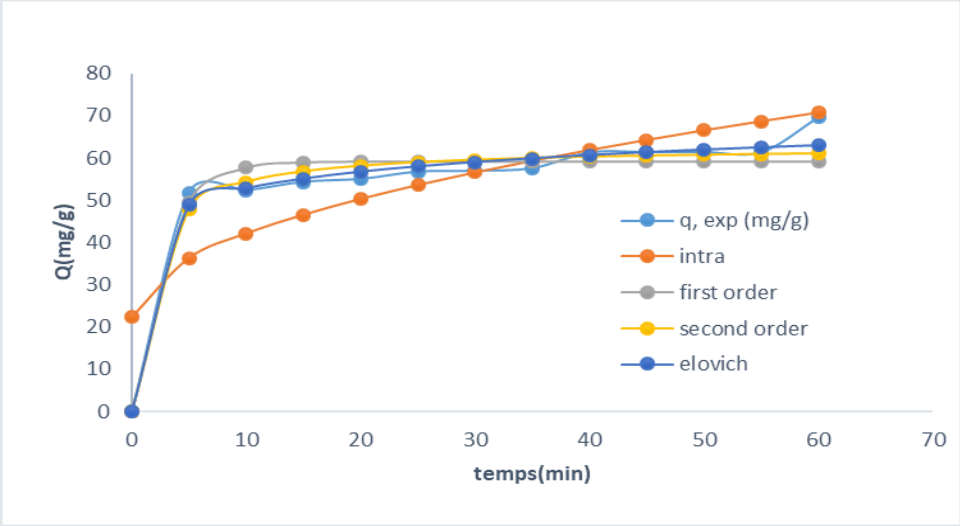

Figure 22: Non-linear representation of kinetic model of IC adsorption

Table 11: Non-linear adsorption kinetic parameter of IC and Cu(II) ions by ACP for different models

Models	**Parameters**	**ADSORBATES**	
		IC	**Cu(II)**
Pseudo-Premier Ordre	Q_e (pred)(mg g^{-1})	59,197	147,710
	K_1 ($mins^{-1}$)	0,364	0,293
	R^2	0,934	0,942
	RMSE	4,383	10,312
	$\chi 2$	3,599	8,160
Pseudo-Second Ordre	Q_e (pred)(mg g^{-1})	62,577	156,994
	K_2 ($mins^{-1}$)	0,010	0,003
	R^2	0,961	0,975
	RMSE	3,411	6,828
	$\chi 2$	2,197	3,725
Elovich	α (mg g^{-1} $mins^{-1}$)	6152,137	4697,888

	β (g. $mins^{-1}$)	0,176	0,062
	R^2	0,979	0,991
	RMSE	2,523	4,029
	$\chi 2$	1,172	1,280
Diffusion Intra-Particulaire	K_{id}	6,242	15,922
	C_i ($mg.g^{-1}$)	22 ,377	52,899
	R^2	0,932	0,943
	RMSE	9,635	22,564
	$\chi 2$	12,370	26,090

It appears from the table 11 that, the Elovich model is best suited to describe the adsorption kinetics of IC and Cu(II) ions on our carbon with regard to its R2 close to unity (0.979 and 0.991 respectively for IC and Cu(II) ions). This model allows us to have the initial rate of adsorption α of (6152,137 and 4697,888 respectively for the IC and the Cu(II) ions) and the constancy of desorption β of (0.176 and 0.062 respectively for the IC and the Cu(II) ions), this allows us to confirm the type of adsorption which is the surface chemisorption of the heterogeneous adsorbent because α> β. Moreover, with regard to the values of chi^2 and RMSE extremely smaller than for other models, we can conclude that it is adequate to describe the adsorption phenomenon.

In view of the Pseudo-First Order and Pseudo-Second Order models, the calculated q_e values are almost equal to those obtained experimentally, but the chi^2 and RMSE values are relatively high. The Pseudo-Second Order model provides information that adsorption takes place at localized sites and there is no interaction between molecules; Adsorption is done in monolayers.

For Table 11, the values of the constant Ci associated with the thickness of the diffusion boundary layer were 22.377 and 52.899 $mg.g^{-1}$ for the CI and Cu(II) ions. These high values indicate that intraparticle diffusion was not the only step controlling the adsorption process. This is confirmed by the low value of R^2 and the high values of chi^2 and RMSE.

IV-CONCLUSION

The Box-Behnken plan gave us the following optimal conditions: impregnation ratio 1.3, temperature 333 °C and time 1 hour. The infrared spectroscopy before adsorption reveals absorption bands in the infrared domain that confirm the presence of hydroxyl groups of phenolic function and carboxylic function that give the surface of carbons an acidic character. This acidic character was also confirmed by the value of pHPCN (3.55) less than 7 which shows the predominance of acid groups. Batch experiments showed that ACP retains IC and Cu(II) ions after 40 and 35 minutes, optimal adsorption pH is 2 and 4.5 with a quantity adsorb at 61.3 and 152.5 mg/g respectively for IC and Cu(II) ions. It appears that the Elovich model better describes the adsorption kinetics of the IC (R^2=0.98) and Cu(II) ions (R^2=0.99), by their R^2 and other parameters. In view of these results, we can say that the adsorption is controlled by a monolayer chemical adsorption for IC and Cu(II) ions and with an energetically heterogeneous surface. The FTIR spectra after adsorption confirm these results with the disappearance and appearance of new peaks revealing chemisorption. Isotherms show that no models are adequate to explain the adsorption mechanism.

ACKNOWLEDGMENT

The authors of this manuscript sincerely thank the entire research team of the physical chemistry laboratory of the University of Yaoundé 1 in Cameroon. They are also thankful to all the different authors whose articles are cited and included in reference of this manuscript.

AUTHORS' CONTRIBUTIONS

All working authors were involved in this work from data collection to the final version of the manuscript.

CONFLICT OF INTEREST

There is no conflict of interest between the different authors of this work.

REFERENCES

- Abega, A V., Ndi, N J., Ngomo,M H., (2015), «The performance of activated carbon based cola nuts shells for the removal of Co(II) and Ni(II) ion from aqueous solution», *Journal of innovative science, Engineering* pp 676-683
- Abo, El Naga., Ahmed O., El Saied., Mohamed., Shaban., Seham, A., El Kady., Fathy Y., (2019), « Fast removal of diclofenac sodium from aqueous solution using sugar cane bagasse-derived activated carbon». *Journal of Molecular Liquids*, 48P https://doi.org/10.1016/j.molliq.2019.04.062
- Ahmad, M.A., Alrozi, R., (2010), « Optimization of preparation conditions for mangosteen peel-based activated carbons for the removal of Remazol Brelliant Bleu R using response surface methodology », *Chemical Engineering Journal* ,**165(3),** p 883-890
- Ahmadi, S., Ganjidoust, H., (2021), « Using banana peel waste to synthetisize BPAC/ZnO nanocomposite for photocatalytic degradation of Acid Blue 25: influential parameter, mineralization, biodegradability studies», *J. Environ. Chem. Eng*.**9(5)**.
- Ahmadi, S., Ganjidoust, H., (2021), «Using banana peel waste to synthesize BPAC/ZnO nanocomposite for photocatalytic degradation of Acid Blue 25: influential parameters, mineralization, biodegradability studies». *J. Environ. Chem. Eng*. 9 (5),
- Ankoro, N. O., Kouotou, D., Lunga P K., Godwin, A T.; Lekene N.R., Ndi N. J., Ketcha M J., (2020), « Effect of doping activated carbon based Ricinodendron Heudelottishells with AgNPs on the adsorption of indigo carmine and its antibacterial properties», Arabian *Journal of Chemistry*, **13(5)**, p 5241-5253.
- Ankoro, N.O., Kouotou, D., Belibi, B. P., Ndi, J.N., Ketcha, J.M., (2016), « Removal of indigo carmine dye (IC) by batch adsorption onto dried cola nut shells and its active carbon from aqueous solution medium », *International Journal of Engineering Sciences and Research Technology* **5(3),** p 874-888.
- Arivoli, S., Nandhakumar, V., Saravanan, S., Sulochana, N., (2009), «adsorption dynamics of copper ion by low cost activated carbon» *Arabian Journal for Science and Engineering*,**34** 11p
- Atheba, G.P., Allou, N B., Dongui, B.K., Kra, D.O., Gbassi, K G., Trokourey, A., (2015), « Adsorption du buttylparabène sur du charbon actif à base des coques de coco provenant de Côte d'ivoire », *International Journal of Innovation and Scientific Research*, vol. **13**, p 530-541
- FAOSTAT., 2020, « Données sur la production mondiale des cultures ».

- Harrache, Z., Abbas, M., Aksil, T et Mohamed, T., (2019), « Thermodynamic and Kinetics Studies on Adsorption of Indigo Carmine from Aqueous Solution by Activated Carbon », *Microchemical Journal*, (**144**), p 180-189.

- Hashem, A.H., Saied, E., Hasanin, M.S., (2020), « Green and ecofriendly bio-removal of methylene blue dye from aqueous solution using biologically activated banana peel waste», *Sustain. Chem. Pharm*
- Jiang, Y., Qin, Z., Liang, F., Li, F., Sun, Y., Wang, X., Ma, P., Song, D., (2021), « Vortex-assisted solid-phase extraction based on metal-organic framework/chitosan functionalized hydrophilic sponge column for determination of triazine herbicides in environmental water by liquid chromatography-tandem mass speectrometry», *J.Chromatogr*

- Koutoou, D., Ngomo, H.M., Bacaoui, A., Yacoubi, A., Ketcha, J.M., (2013), «Optimization of activated carbons prepared by H_3PO_4 and steam activation of oil palm shell», *journal of chemistry* 10p

- Lékéné, N.R.B., Ndi N. J., Rauf, A., Kouotou, D., Belibi, B. P.D., Bhanger, M. I., Ketcha, M.J., (2018), « Optimazation conditions of activated carbon based Egusi (Cucumeropsis mannii Naudin) seed shells for nitrite ions removal from wastewater », *American Journal of Analytique Chemistry* **(9)**, pp: 439-463.

- Leon, O., Munoz-Bonilla, A., Soto, D., Perez, D., Rangel, M., Colina, M., Fernandez García, M., (2018), «Removal of anionic and cationic dyes with bioadsorbent oxidized chitosans», *Carbohydr Polym* **194** pp: 375-383.

  https://doi.org/10.1016/j.carbpol.2018.04.072.

- Li, H., An, N., Liu, G., Li, J., Liu, N., Jia, M., Zhang, W., Yuan, X., (2016), «Adsorption behaviors of methyl orange dye on nitrogen-doped mesoporous carbon materials», *Journal of Colloid Interface Sci*. **466**, pp:343-351.

  https://doi.org/10.1016/j.jcis.2015.12.048

- Mashile, G.P., Mpupa, A., Nomngongo, P.N., (2021), «Magnetic mesoporous carbon/ β-cyclodextrin–chitosan nanocomposite for extraction and preconcentration of multi-class emerging contaminant residues in environmental samples», *Nanomaterials* **11 (2)**, pp:1–16

- Mohammad-Khah, A et Ansari, R., (2009), «Activated charcoal: preparation, characterization and applications », A review article. *International journal of Chemical and Technology Research*, (1), p 859-864.

- Mohammed Jaafar Ali Alatabe., Zainab T Al-Sharify., (2019), «Utilization of low cost adsorbents for the adsorption process of lead ions», *International Journal of Modern Research in Engineering and Technology* **4** 22p

- Mthombeni, N.H., Mbakop, S., Ray, S.C., Leswifi, T., Ochieng, A., Onyango, M.S., (2018), « Highly efficient removal of chromium (VI) through adsorption and reduction: a column dynamic study using magnetized natural zeolite-polypyrrole composite», *Journal of Environnemental Chemical Engineering*, **6(4)**, p 4008-4017.

- Ndifor-Angwafor, N G., Tiostop. I H., Thuifon. R D., Ngakou.C., Bopda. A., KamdemA T., Anagho. S G., (2017), « Biosorption of amaranth red in aqueous solution

onto treated and untreated lignocellulosic materials (pineapplepeelings and coconut shells) », *Journal of materials and environmental science* **vol 8** pp 4199-4212

- Ngaha, M.C.D., Njanja. E., Doungmo. G., Kamdem. T., Tonleu. I.K., (2019), « Indigo carmine and 2,6-Dichlorophenolindophenol removal using cetyltrimethylammonium bromide-modified palm oil fiber: Adsorption isotherm and mass transfer kinetics» *International Journal of Biomaterials* 19p

- Ousmaila, S.M., Adamou, Z., Ibrahim, D., Ibrahim, N., (2016), « Préparation et caractérisation de charbons actifs à base de coques de noyaux de Balanites Eagyptiaca et de Zizyphus Mauritiana », *Journal Social Ouest-Africa Chimie*., **041** pp 59-67.

- Rashid, R., Shafiq, I., Iqbal, M J.; Shabir, M., Akhter, P., Hamayun, M. H., Ahmed, A., Hussain, M., (2021), « Synergistic effect of NS co-doped TiO_2 adsorbent for removal of cationic dyes», *J. Environ. Chem. Eng.* https://DOI.org/10.1016/j.jece.2021.105480.

- Wong, S., Ngadi, N., Hassan, O., (2018), « Recent advances in applications of activated carbon from biowaste for waste wastewater treatment»: a short review. *J.Clean Prod* **175**, pp: 361-375

- Zhu, G.Z., Deng, X.L., Hou, M., Sun, K., Zhang, Y.P., Li, P., (2016), « comparative study on characterization and adsorption properties of activated carbons by phosphoric acid activation from corncob and its acid and alkaline hydrolysis residues», *Fuel Processing Technology* (144), p 255-256.

- Zulfiqar M., Samsudin M.F.R., Sufian S., (2019), «Modelling and optimization of photocatalytic degradation of phenol via TiO_2 nanoparticles: An insight into response surface methodology and artificial neural network». *Journal of Photoch. Photobio*., **384**, pp112-398